Supporting Information

High-Conductivity, Low-Temperature Sintering-Compatible NASICON Solid Electrolyte for Enhanced Compositing with Hard Carbon Electrode in All-Solid-State Batteries

Bowei Xun[a], Yukio Sato[b], Jian Wang[a], George Hasegawa[c], Hirofumi Akamatsu[a], Katsuro Hayashi[a*]

[a]Department of Applied Chemistry, Graduate School of Engineering, Kyushu University, 744 Motooka, Nishi-ku, Fukuoka 819-0395, Japan

[b]Research and Education Institute for Semiconductors and Informatics, Kumamoto University, 2-39-1 Kurokami, Chuo-ku, Kumamoto 860-8555, Japan

[c]Institute of Materials and Systems for Sustainability, Nagoya University, Furo-cho, Chikusa-ku, Nagoya 464-8601, Japan

*Corresponding author: e-mail: k.hayashi@cstf.kyushu-u.ac.jp

Table of Contents:

Experimental Section

Preparation of NZSP-based electrolyte powder and sinter

Regent grade powders of Na_3PO_4 (Purity of > 98.0%; Kishida Chemical Company, Japan), ZrO_2 (99.9%; Kojundo Chemical Laboratory, Japan), SiO_2 (99.9%; Kojundo) Na_2CO_3 (> 99.0%; Kojundo), and Al_2O_3 (99.9%; Kojundo) were weighed according to ratios for $Na_3Zr_2Si_2P_3O_{12}$ (NZSP), $Na_{3.4}Zr_2Si_{2.35}P_{0.65}O_{12}$ ($NZS_{2.35}P$), and $Na_{3.4}Zr_{1.95}Al_{0.05}Si_{2.35}P_{0.65}O_{12}$ ($NZAS_{2.35}P$). These powders were put in a zirconia pot with zirconia balls (ϕ 4 mm, YTZ; Nikkato, Japan) and ethanol as a solvent, and planetary ball milling (PBM) was performed at 200 rpm for 2 h using a Fritsch P-6 (Friche, Germany). After drying, the mixtures were calcined at 1100 °C for 12 h in air. The calcined products were ground into fine powders by PBM using zirconia balls and ethanol at 250 rpm for 18 h, followed by drying.

As sintering aid additives, mixtures of Na_2CO_3 and B_2O_3 (99.9%; Kishida) powders with molar ratios of 1:3 ($1Na_2CO_3 + 3B_2O_3$, referred to as NB_3), 1:2 (NB_2), 1:1 (NB), 2:1 (N_2B), and 3:1 (N_3B), as well as $Na_2B_4O_7$ (99.0%; Kishida) were used. These additives were mixed with calcined electrolyte powders of NZSP, $NZS_{2.35}P$ or $NZAS_{2.35}P$ in proportions ranging from (y =) 0 to 20 wt% of the weight of electrolytes. The mixtures were processed by PBM for at 250 rpm 6 h, dried and then passed through a 57 μm sieve. The finalized powders were used as a precursor for bulk sintering or as an electrolyte component for composite electrodes. For example, a sample containing $Na_{3.4}Zr_{1.95}Al_{0.05}Si_{2.35}P_{0.65}O_{12}$-10wt% of $2Na_2CO_3 + 1B_2O_3$ mixture is referred to as $NZAS_{2.35}P$-$10N_2B$.

For the preparation of bulk electrolyte, each powder was uniaxially pressed into disks with a diameter of 15 mm and a thickness of 1.0 mm at 40 MPa, followed by cold-isostatic pressing at 250 MPa. These disks were then buried in the calcined powder, and sintered at 900 °C for 12 h in air.

Preparation of hard carbon sphere and fabrication of composite electrode

Powder of hard carbon (HC) with a spherical shape were prepared by hydrothermal synthesis of resorcinol-formaldehyde (RF) resin spheres as a precursor, followed by a thermal carbonization.[1] First, a mixture of 0.1 mL ammonia aqueous solution (25 wt%NH_4OH, Kishida Chemical), 8 mL ethanol (99%, Japan Alcohol Trading Company), and 20 mL deionized water was stirred for more than 1 h, and second 0.2 g resorcinol (99%, Sigma-Aldrich) and 0.28 mL formaldehyde solution (37 wt%, Sigma-Aldrich, USA) were added into the solution and further stirred for 24 h at 30 °C. Next, the mixture was transferred into a Teflon-lined autoclave, and warmed at 100 °C for 24 h in a constant-temperature oven. The reddish-brown solid product (RF resin) was separated by a high-speed centrifuge (MX-205, TOMY, Japan) by repeating the process 5 times. After drying at 100 °C for 48 h, the RF resin was first heated at 350 °C for 2 h with a heating rate of 1 °C min^{-1}, and then calcined at 1300 °C for 4 h with a heating rate of 1 °C min^{-1} in an N_2 atmosphere, resulting in the black hard carbon spheres (HCS).

For the preparation of the composite electrode, the HCS powder, and the $NZAS_{2.35}P$-10NB powder, polyvinyl butyral (PVB, Fujifilm, Japan) as a binder, and ethanol as a solvent were mixed in a weight ratio of 6:8:3:300. This mixture was ultrasonicated using a US-103 (SND Company, Japan) for 1 h to form a suspension. A sintered $NZAS_{2.35}P$-10NB disk with 11.0 mm in diameter and 0.90 mm in thickness was used as a substrate. The suspension was then applied to the substrate using a spin-coater (K-35951, Kyowa Riken, Japan) at 2800 rpm, with totally 15 drops (~10 μL per drop). The mass loading of HCS was 1.4–1.8 × 10^{-4} g on an area of 0.60 cm^2. After coating, the disk was heated at 330 °C for 5 h in air with a heating rate of 1 °C min^{-1} to gradually remove the PVB. Finally, the disk

was heated at 900 °C for 0.5 h in an N_2 atmosphere using an alumina-tube furnace.

Sample characterization

The density of the ceramic sample was evaluated using the Archimedes method. X-ray diffraction (XRD) analysis was carried out using a D8 ADVANCE (Bruker AXS, Germany) equipped with a Bragg-Brentano diffractometer and a Cu Kα radiation source. Rietveld refinement of the XRD pattern was performed using TOPAS software (Bruker). The microstructure and elemental distributions were analyzed with a scanning electron microscope equipped with an energy-dispersive X-ray spectrometer (SEM-EDS, JCM-700, JEOL, Japan). Samples for scanning transmission electron microscopy (STEM) were prepared using a focused ion beam system (NB5000, Hitachi High-Tech Co., Japan). STEM observations were conducted using a JEM-ARM200F NEOARM (JEOL Ltd., Japan) at an acceleration voltage of 60 kV, equipped with an EDS (JED-2300T, JEOL Ltd., Japan), to obtain structural and chemical compositional information.

Electrochemical measurements

For electrochemical impedance spectroscopy (EIS), Au electrodes with a thickness of 25 nm were deposited on both sides of a sample using a vacuum evaporator (VTC-YAN350, VTECH, Japan). The sample was installed in an assembling-type hermetic cell and placed in a constant temperature chamber, in which the temperature was varied from −40 to 80 °C. EIS was measured using a VMP3 (Biologic, France) with a modulation amplitude of 20 mV over a frequency range from 1 MHz and 100 mHz. The obtained spectra were analyzed through an equivalent circuit fitting using RelaxIS3 software (rhd instruments, Germany).

For a half-cell measurement, a Na counter electrode (99.9%, Sigma-Aldrich) was mechanically attached to one side of a sample by pressure application of 1 MPa and installed in the assembling-type cell in an Ar-filled dry box. Galvanostatic charge-discharge property was measured using a VMP3 in a voltage cut off range from 0.01 to 2.5 V (or 3.0 V) and a current density range from 6 to 60 μA cm^{-2} at 25 °C.

Table S1. Summary of Ionic Conductivities, Sintering Conditions and Synthesis Methods of NZSP-Based Solid Electrolytes.

Chemical composition	Sintering condition	Method	σ_{RT} (10^{-3} S cm^{-1})	Reference
$Na_{3.256}Mg_{0.128}Zr_{1.872}Si_2PO_{12}$	1300 °C/ 24 h	Solid-state reaction	2.7	[2]
$Na_{3.1}Zr_{1.95}Mg_{0.05}Si_2PO_{12}$	1260 °C/ 16 h	Solid-state reaction & Mechanochemical synthesis	3.5	[3]
$Na_{3.3}Zr_{1.9}Nb_{0.1}Si_{2.4}P_{0.6}O_{12}$	1260 °C/5 h	Solution-assisted solid-state reaction	5.5	[4]
$Na_{3.4}Zr_2Si_{2.4}P_{0.6}O_{12}$	1260 °C/5 h	Solution-assisted solid-state reaction	5.0	[5]
$Na_{3.4}Sc_{0.4}Zr_{1.6}(SiO_4)_2(PO_4)$	1260 °C/6 h	Solution-assisted solid-state reaction	4.0	[6]
$Na_{3.4}Zr_{1.9}Zn_{0.1}Si_{2.2}P_{0.8}O_{12}$	1250 °C pure oxygen	Solid-state reaction	5.3	[7]
$Na_{3.3}Zr_{1.7}La_{0.3}Si_2PO_{12}$	1200 °C/ 24 h	Sol-gel method	3.4	[8]
$Na_3Zr_2Si_2PO_{12}$-5 wt% Na_2SiO_3	1175 °C/10 h	Solid-state reaction	1.5	[9]
$Na_3Zr_2Si_2PO_{12}$-0.75 wt% CuO	1150 °C/10 h	Solid-state reaction	1.7	[10]
$Na_3Zr_2Si_2PO_{12}$-5 wt% $Na_2Si_2O_5$	1150 °C/12 h	Solid-state reaction	1.7	[11]
$Na_3Zr_2Si_2PO_{12}$-5 wt% Na_2SiO_3	1100 °C/12 h	Solid-state reaction	1.3	[12]
$Na_3Zr_2Si_2PO_{12}$-0.7 mol NaF	1100 °C/24 h	Solid-state reaction	1.4	[13]
$Na_{3.1}Y_{0.1}Zr_{1.9}Si_2PO_{12}$-1 wt% Bi_2O_3	1100 °C/6 h	Solid-state reaction	1.2	[14]
$Na_3Zr_2Si_2PO_{12}$-5 wt% 60Na_2O-10Nb_2O_5-30P_2O_5	1100 °C /4 h	Tape casting	0.44	[15]
$Na_3Zr_2Si_2PO_{12}$-0.2 mol $(ZnO)_2$–$(B_2O_3)_3$	1000 °C/12h	Solid-state reaction	1.6	[16]
$Na_3Zr_2Si_2PO_{12}$-5 wt% 60Na_2O-10Nb_2O_5-30P_2O_5	1045 °C /0.5h	Spark plasma sintering (SPS)	1.0	[17]
$Na_3Zr_2Si_2PO_{12}$-$NaPO_3$	1000 °C/10 h	Solid-state reaction	1.8 (100 °C)	[18]
$Na_3Zr_2Si_2PO_{12}$-10 wt% $Na_2B_4O_7$	1000 °C/10 h	Solid-state reaction	1.7	[19]
$Na_{3.3}La_{0.3}Zr_{1.7}Si_2PO_{12}$-3 wt% $Na_2B_4O_7$	950 °C/6 h	Solid-state reaction	1.8	[20]
$Na_3Zr_2Si_2PO_{12}$-10 wt% 60Na_2O-10Nb_2O_5-30P_2O_5	900 °C/10 min	Solid-state reaction	0.12	[21]
$Na_3Zr_2Si_2PO_{12}$-4.8 wt% Na_3BO_3	900 °C/10 h	Solid-state reaction	1.4	[22]
$Na_3Zr_2Si_2PO_{12}$-9.1 wt% Na_3BO_3	700 °C/20 h	Solid-state reaction	0.1	[23]
$Na_{3.1}Zr_{1.95}Mg_{0.05}Si_2PO_{12}$-20 wt% $NaBO_2{\cdot}4H_2O$	400 °C/10 min/102 MPa	Spark plasma sintering (SPS)	0.33	[24]
$Na_3Zr_2Si_2PO_{12}$-10 wt% NaOH	375 °C/3 h/350 MPa	Cold sintering process	0.2	[25]
$Na_{3.4}Zr_{1.95}Al_{0.05}Si_{2.35}P_{0.65}O_{12}$	1270 °C/12 h	Solid-state reaction	6.0	Our work[26]
$Na_{3.4}Zr_{1.95}Al_{0.05}Si_{2.35}P_{0.65}O_{12}$ +10 %wt (Na_2CO_3+B_2O_3)	900 °C/12 h	Solid-state reaction	4.5	This work

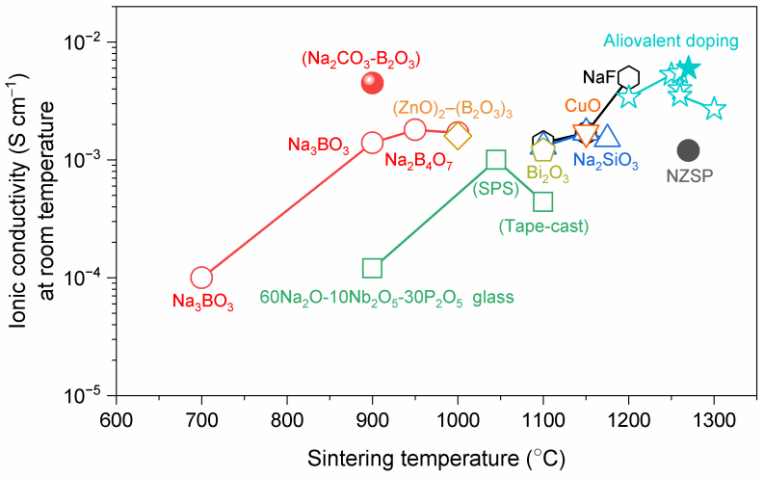

Fig. S1. Ionic conductivities at room temperature plotted against sintering temperature for NZSP-based electrolytes, as listed in Table S1. A general trend of decreasing the conductivity is observed with decreasing the sintering temperature. The data from the present study is plotted by the filled red circle.

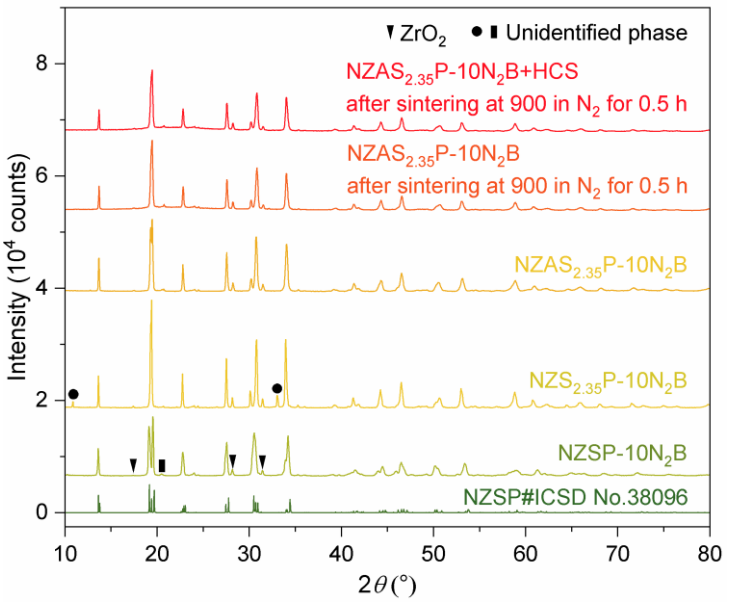

Fig. S2. Powder XRD patterns for NZSP-10N_2B, $NZS_{2.35}$P-10N_2B, $NZAS_{2.35}$P-10N_2B sintered at 900 °C, and $NZAS_{2.35}$P-10N_2B with mixture of hard carbon sphere (HCS) after sintering at 900 °C in N_2 for 0.5 h. These samples predominantly consist of NASICON-type crystals, with minor secondary phases of ZrO_2 and unidentified phase. The patterns of the sample after sintering at 900 °C in N_2 for 0.5 h show the main peaks of NASICON with minimal changes, indicating a chemical stability of the composite electrode after co-sintering.

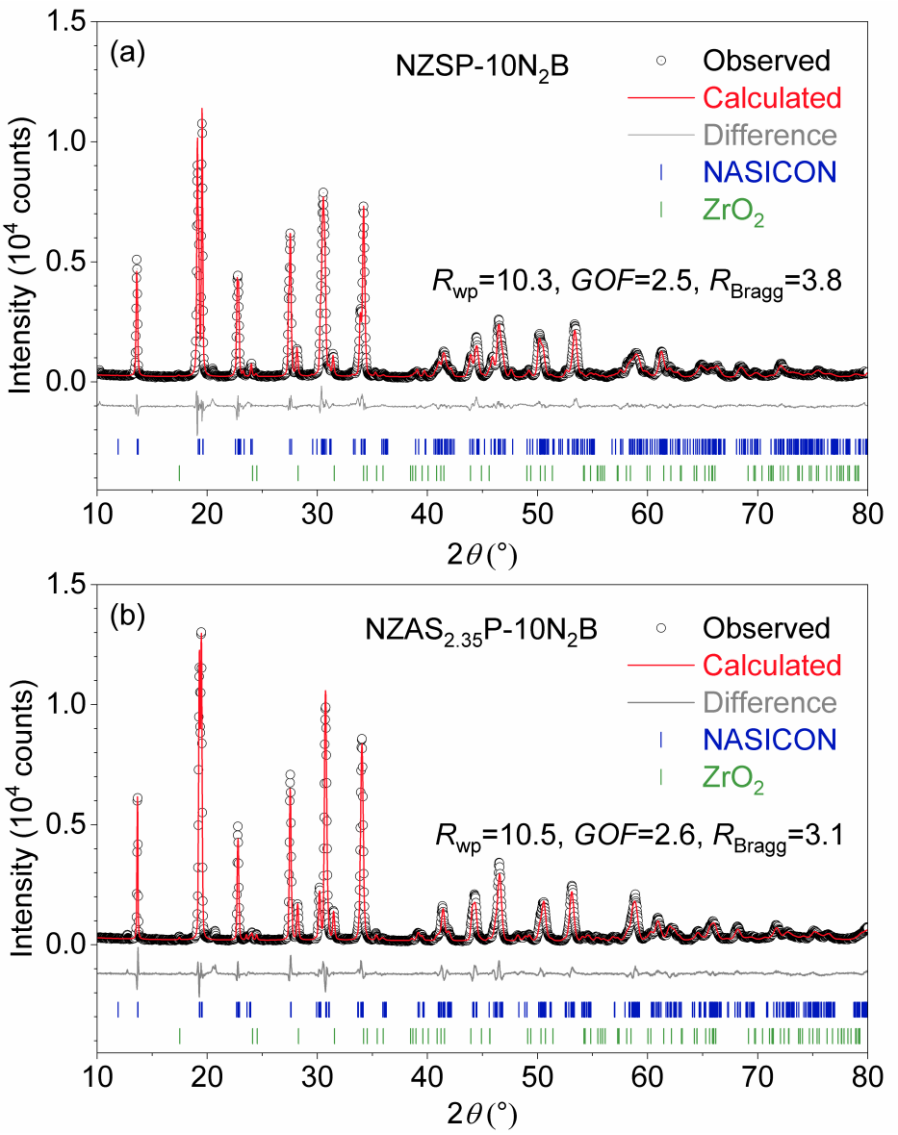

Fig. S3. Cu-Kα XRD patterns and Rietveld refinement results for (a) NZSP-10N_2B and (b) $NZAS_{2.35}$P-10N_2B sintered at 900 °C. Both patterns were refined by monoclinic (space group *C*2/*c*) NASICON phase and monoclinic ($P2_1/c$) ZrO_2 phase. The ZrO_2 content was estimated to be 4.2 and 5.2 wt%, respectively. The refined crystallographic parameters for the NASICON phases are listed in Tables S2 and S3, respectively.

Table S2. Rietveld Refined Parameters for $Na_3Zr_2Si_2PO_{12}$-10 wt% ($2Na_2CO_3 + B_2O_3$).

Space group: *C*2/*c*

Cell parameters: a = 15.6972(8), b = 9.0762(5), c = 9.2167(4) Å, β = 124.090(3)°, and V = 1087.466(103) Å^3

Site	Wyckoff	x	y	z	g	U_{iso} (Å^2)
Na1	4d	1/4	1/4	1/2	0.81	0.2503
Na2	4e	1/2	0.893(3)	1/4	1	0.0086
Na3	8f	0.8367(19)	0.082(3)	0.815(3)	0.6	0.054
Zr1	8f	0.1017(3)	0.2486(9)	0.0556(3)	1	0.0020
Si1	4e	0	0.028(2)	1/4	0.67	0.0006
Si2	8f	0.3538(12)	0.111(2)	0.255(2)	0.67	0.0201
P1	4e	0	0.028(2)	1/4	0.33	0.0006
P2	8f	0.3538(12)	0.111(2)	0.255(2)	0.33	0.0201
O1	8f	0.1591(15)	0.402(2)	0.254(2)	1	0.0012
O2	8f	0.4376(15)	0.466(2)	0.093(3)	1	0.0049
O3	8f	0.2647(18)	0.166(3)	0.223(3)	1	0.0141
O4	8f	0.3736(14)	0.147(2)	0.088(2)	1	0.0132
O5	8f	0.4412(15)	0.167(2)	0.436(3)	1	0.0069
O6	8f	0.0831(17)	0.129(2)	0.248(2)	1	0.0018

Table S3. Rietveld Refined Parameters for $Na_{3.40}Zr_{1.95}Al_{0.05}Si_{2.35}P_{0.65}O_{12}$-10 wt% ($2Na_2CO_3 + B_2O_3$).

Space group: *C*2/*c*

Cell parameters: a = 15.809(1) Å, b = 9.100(1) Å, c = 9.219(1) Å, β = 125.039(6)°, and V = 1085.859(182) Å^3.

Site	Wyckoff	x	y	z	g	U_{iso} (Å^2)
Na1	4d	1/4	1/4	1/2	0.87(3)	0.2419
Na2	4e	1/2	0.913(4)	1/4	1	0.0152
Na3	8f	0.811(3)	0.080(5)	0.724(4)	0.76(3)	0.0431
Zr1	8f	0.1047(5)	0.2499(10)	0.0593(3)	0.975	0.0027
Al1	8f	0.1047(5)	0.2499(10)	0.0593(3)	0.975	0.0027
Si1	4e	0	0.049(4)	1/4	0.783	0.0015
Si2	8f	0.3593(17)	0.100(2)	0.269(3)	0.783	0.0066
P1	4e	0	0.049(4)	1/4	0.217	0.0015
P2	8f	0.3593(17)	0.100(2)	0.269(3)	0.217	0.0066
O1	8f	0.186(2)	0.440(3)	0.305(3)	1	0.0013
O2	8f	0.456(2)	0.376(2)	0.092(3)	1	0.0013
O3	8f	0.243(2)	0.183(3)	0.222(3)	1	0.0013
O4	8f	0.329(2)	0.119(3)	0.056(4)	1	0.0013
O5	8f	0.445(2)	0.177(3)	0.409(4)	1	0.0013
O6	8f	0.090(3)	0.128(3)	0.251(4)	1	0.0013

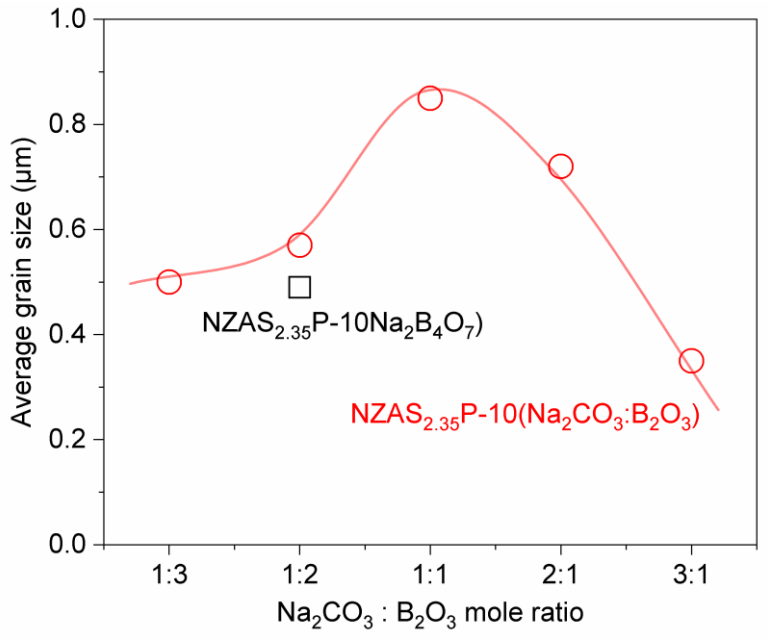

Fig. S4. Average grain size determined by the line intercept analysis of SEM images. The grain size shows slight increase with the higher proportion of B_2O_3, peaking at the ratio of 1:1.

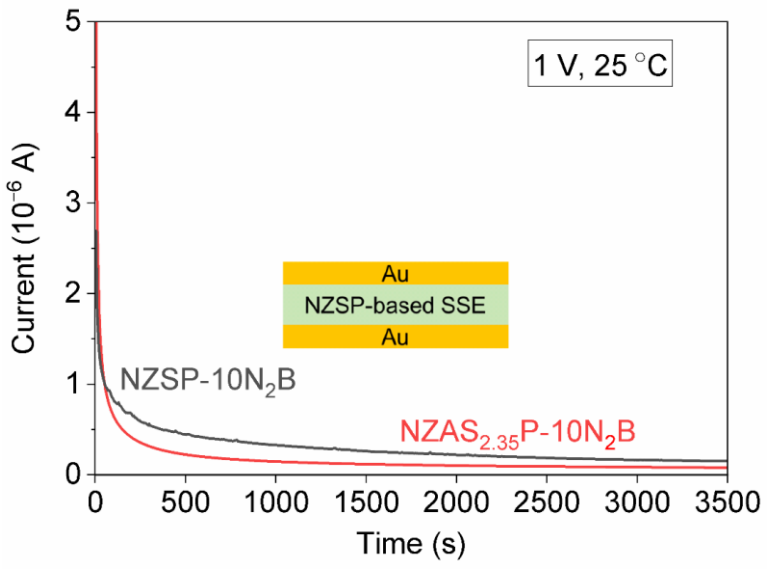

Fig. S5. Chronoamperometry of Au | $NZSP\text{-}10N_2B$ | Au and Au | $NZAS_{2.35}P\text{-}10N_2B$ | Au cells measured with an external voltage application of 1 V at 25 °C. The partial electronic conductivities in $NZSP\text{-}10N_2B$ and $NZAS_{2.35}P\text{-}10N_2B$ are estimated to be 3.5×10^{-8} and 1.8×10^{-8} S cm^{-1}, respectively. The electronic conductivity is approximately 5 orders of magnitude lower than the total conductivities.

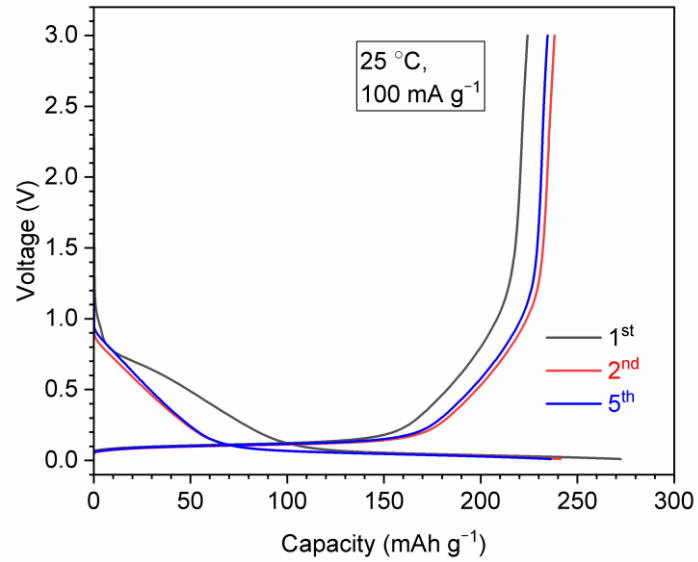

Fig. S6. Charge-discharge properties of the HCS electrode in an organic liquid electrolyte system. The HCS electrode was prepare by mixing the HCS with carbon black as a conductive aid and carboxymethylcellulose sodium (CMC-Na) as a binder, followed by application to an Al foil. The beaker cell comprised of the HCS electrode as the working electrode, metallic Na as both the reference and counter electrodes, and 1 M $NaPF_6$ in ethylene carbonate/dimethyl carbonate (EC/DMC) 1:1 mixture as the electrolyte.

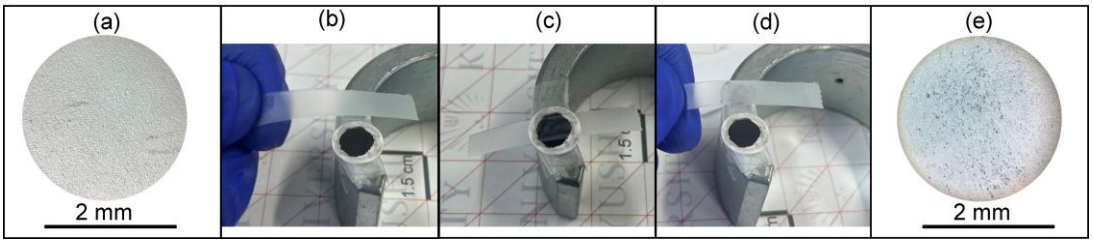

Fig. S7. Scotch tape test to evaluate the adhesion of the sintered HCS-$NZAS_{2.35}P$-$10N_2B$ composite thick film to the $NZAS_{2.35}P$-$10N_2B$ substrate. (a) Photograph of the adhesive tape (Scotch® Magic™ Tape 810 manufactured by 3M) in its original pristine state. (b-d) Images showing the sample and the tape in their initial condition, during adhesion, and after peering off the tape. (e) Magnified image of the tape after peering. No delamination of the composite thick film was observed, although a small portion of surface HCS particles was detached.

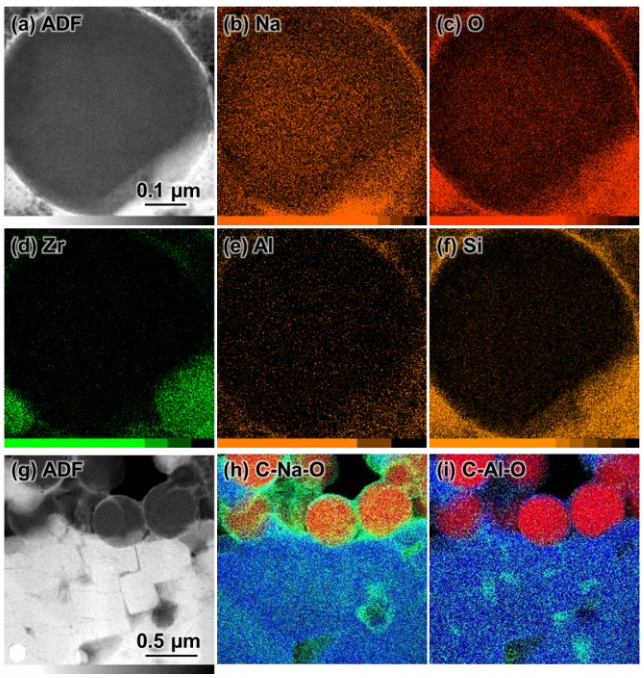

Fig. S8. STEM-EDS analyses for the cross section of HCS-$NAS_{2.35}P$-10N2B composite electrode on $NAS_{2.35}P$-$10N_2B$ ceramic substrate. (a-f) A HCS particle: (a) HAADF image; and (b-f) EDS elemental maps for (b) Na, (c) O (blue), (d) Zr, (e) Al, and (f) Si K-line signals. (g-i) A region including HCS and polycrystalline electrolyte: (g) HAADF image; and (h-i) composite EDS maps for (h) C (red), Na (green), and O (blue), and (i) C (red), Al (green), and O (blue) K-line signals.

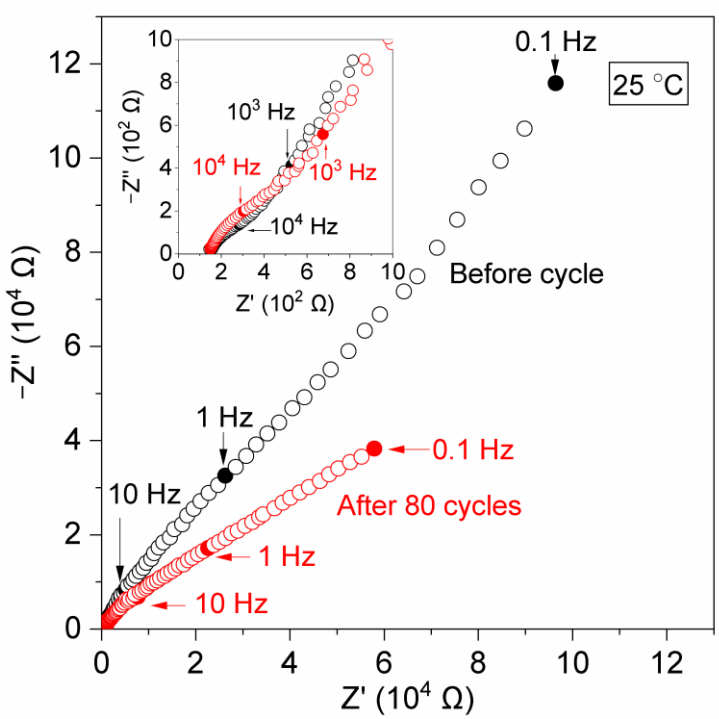

Fig. S9. The Nyquist plot of the EIS measurement for Na | $NZAS_{2.35}P$-$10N_2B$ | HCS-$NZAS_{2.35}P$-$10N_2B$ cell before and after charge-discharge 80 cycles. The inset highlights the high-frequency spectra, corresponding to the impedance of the electrolyte and electrolyte-electrode interfaces, showing minimal changes in impedance after 80 cycles. The main figure focuses on the low-frequency spectra, associated with diffusion processes in the composite electrode, which exhibit a decrease in capacitance and resistance at given frequencies. This change is primarily attributed to alterations in the electrochemical properties of the HCSs.

References

1 J. Liu, S. Z. Qiao, H. Liu, J. Chen, A. Orpe, D. Zhao and G. Q. (Max) Lu, *Angew. Chem. Int. Ed.*, 2011, **50**, 5947–5951.

2 M. Samiee, B. Radhakrishnan, Z. Rice, Z. Deng, Y. S. Meng, S. P. Ong and J. Luo, *J. Power Sources*, 2017, **347**, 229–237.

3 S. Song, H. M. Duong, A. M. Korsunsky, N. Hu and L. Lu, *Sci. Rep.*, 2016, **6**, 32330.

4 Y. Liu, L. Liu, J. Peng, X. Zhou, D. Liang, L. Zhao, J. Su, B. Zhang, S. Li and N. Zhang, *J. Power Sources*, 2022, **518**, 230765.

5 Q. Ma, C.-L. Tsai, X.-K. Wei, M. Heggen, F. Tietz and J. T. S. Irvine, *J. Mater. Chem. A*, 2019, **7**, 7766–7776.

6 Q. Ma, M. Guin, S. Naqash, C.-L. Tsai, F. Tietz and O. Guillon, *Chem. Mater.*, 2016, **28**, 4821–4828.

7 J. Yang, G. Liu, M. Avdeev, H. Wan, F. Han, L. Shen, Z. Zou, S. Shi, Y.-S. Hu and C. Wang, *ACS Energy Lett.*, 2020, **5**, 2835–2841.

8 Z. Zhang, Q. Zhang, J. Shi, Y. S. Chu, X. Yu, K. Xu, M. Ge, H. Yan, W. Li and L. Gu, *Adv. Energy Mater.*, 2017, **7**, 1601196.

9 J. A. S. Oh, L. He, A. Plewa, M. Morita, Y. Zhao, T. Sakamoto, X. Song, W. Zhai, K. Zeng and L. Lu, *ACS Appl. Mater. Interfaces*, 2019, **11**, 40125–40133.
10 Z. Sun, L. Li, C. Sun, Q. Ni, Y. Zhao, H. Wu and H. Jin, *Nano Lett.*, 2022, **22**, 7187–7194.
11 B. Santhoshkumar, M. B. Choudhary, A. K. Bera, S. M. Yusuf, M. Ghosh and B. Pahari, *J. Am. Ceram. Soc.*, 2022, **105**, 5011–5019.
12 H. Wang, G. Zhao, S. Wang, D. Liu, Z. Mei, Q. An, J. Jiang and H. Guo, *Nanoscale*, 2022, **14**, 823–832.
13 S. He, Y. Xu, Y. Chen and X. Ma, *J. Mater. Chem. A*, 2020, **8**, 12594–12602.
14 R. J. Miao, X. G. Cao, W. G. Wang and H. Y. Zhang, *Ceram. Int.*, 2021, **47**, 17455–17462.
15 K. Okubo, H. Wang, K. Hayashi, M. Inada, N. Enomoto, G. Hasegawa, T. Osawa and H. Takamura, *Electrochim. Acta*, 2018, **278**, 176–181.
16 C. Wang, C. Sun, Z. Sun, B. Wang, T. Song, Y. Zhao, J. Li and H. Jin, *J. Mater. Chem. A*, 2022, **10**, 5280–5286.
17 H. Wang, K. Okubo, M. Inada, G. Hasegawa, N. Enomoto and K. Hayashi, *Solid State Ionics*, 2018, **322**, 54–60.
18 Y. Ji, T. Honma and T. Komatsu, *Materials*, 2021, **14**, 3790.
19 Y. Zhao, C. Wang, Y. Dai and H. Jin, *Nano Energy*, 2021, **88**, 106293.
20 Z. Wang, Z. Wang, M. Li, C. Tang, K. Yu, P. Lv and W. Wei, *Solid State Ionics*, 2023, **396**, 116229.
21 T. Honma, M. Okamoto, T. Togashi, N. Ito, K. Shinozaki and T. Komatsu, *Solid State Ionics*, 2015, **269**, 19–23.
22 K. Noi, K. Suzuki, N. Tanibata, A. Hayashi and M. Tatsumisago, *J. Am. Ceram. Soc.*, 2018, **101**, 1255–1265.
23 K. Suzuki, K. Noi, A. Hayashi and M. Tatsumisago, *Scripta Mater*, 2018, **145**, 67–70.
24 D. Kutsuzawa, *ACS Energy Lett.*, 2024, **9**, 4347–4352.
25 Z. M. Grady, K. Tsuji, A. Ndayishimiye, J. Hwan-Seo and C. A. Randall, *ACS Appl. Energy Mater.*, 2020, **3**, 4356–4366.
26 B. Xun, J. Wang, Y. Sato, S. Jia, S. Ohno, H. Akamatsu and K. Hayashi, *Adv. Energy Mater*., 2024, 2402891.